NANO LETTERS

pubs.acs.org/NanoLett
Letter

Defectless and Uniform Single-Crystallite Dispersions of Sustainable Wood Nanocellulose with a Regulated Right-Handed Twist Periodicity

Tomoki Ito, Kazuho Daicho, Shuji Fujisawa, Tsuguyuki Saito,* and Kayoko Kobayashi*

Cite This: *Nano Lett.* 2025, 25, 6085−6091

ABSTRACT: Controlling the quality of cellulose nanofibers (CNFs), such as dispersibility and defects, is crucial for fully exploiting sustainable wood-derived CNFs. The dispersibility of CNFs is now tailorable, whereas the defects are still uncontrollable. This study is the first to demonstrate defect suppression through the selection of raw material species and the chemical pretreatment for cellulose. Two raw materials of softwood pulp and holocellulose are chosen from the perspective of the nanoscale supramolecular structure of plant celluloses. These two materials are subjected to regioselective surface oxidation using 4-acetamido-2,2,6,6-tetramethylpiperidinyl-1-oxyl as a catalyst at two different pHs to prepare four types of CNFs. Through statistical analysis of the CNF morphology using atomic force microscopy (AFM) image processing, we found a process yielding defectless CNF dispersions comprising uniform single crystallite units of cellulose. Wavelet transform analysis of AFM height profiles further revealed that the defectless CNFs exhibit regulated twist periodicity along much of their length.

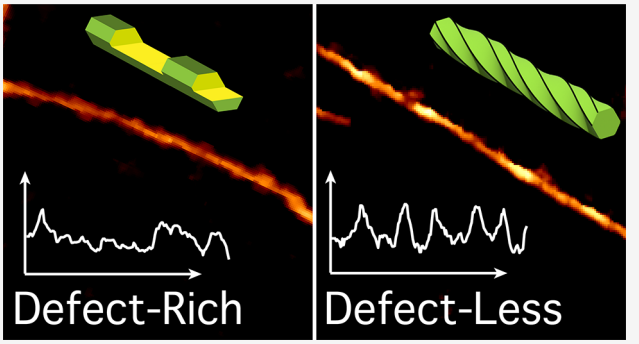

KEYWORDS: *cellulose nanofibers, defects, twist, statistical analysis, wavelet transform*

Cellulose nanofibers (CNFs) are dispersions of the slender crystallite units of plant cellulose that are histologically defined as microfibrils, and they are produced via wet disintegration of cell wall cellulose.[1] CNFs have excellent mechanical and thermal properties, and their commercialization for diverse applications is underway toward the realization of a low-carbon society. However, there still remain unknown structural aspects of single CNFs, which need to be revealed for accurate design of the functionality of CNFs or their composites with other materials. One of these aspects is defects: CNFs have defects such as dents and kinks, but strategies to control these CNF defects have not yet been established.[2−4]

The defect structure of CNFs critically influences their mechanical properties and biodegradability. Ciesielski et al. showed that kink defects promote enzymatic hydrolysis, affecting degradation, and Martoïa et al. demonstrated that kinks reduce the elastic modulus of CNF-based nanopapers.[5,6] Minimizing defects is therefore essential for enhancing CNF durability and performance in nanocomposites. In our previous study, we suggested that the dents on the surface of CNFs are the initial defects, which propagate into further defects such as kinks and mechanical breakdown into short CNFs.[3] Therefore, in this study, we focus on these dents as the "defects" and explore ways to reduce them.

The dispersibility of CNFs depends on the raw material species.[7−9] Softwood bleached kraft pulp is a common raw material used in CNF production. Bleached kraft pulps contain approximately 10−15% of amorphous hemicelluloses, and most microfibrils are segregated from hemicelluloses in the pulp and densely aggregated.[10] The CNFs derived from bleached kraft pulps are thus thick bundles of microfibrils when they are produced via disintegration by a mechanical process alone.[11] Holocellulose has been proposed to have structural advantages as a raw material for providing fine CNFs.[12,13] Holocellulose contains approximately 20−40% hemicelluloses, which cover microfibrils and suppress their agglomeration.[14] However, even from holocellulose, mechanical disintegration alone cannot produce truly uniform CNFs dispersed as single microfibril units with a width of approximately 2−3 nm.[15] To produce CNF dispersions of microfibril units, an oxidative reaction using 2,2,6,6-tetramethylpiperidinyl-1-oxyl (TEMPO)

Received: December 18, 2024
Revised: March 17, 2025
Accepted: March 19, 2025
Published: April 7, 2025

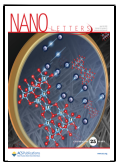

https://doi.org/10.1021/acs.nanolett.4c06483
Nano Lett. 2025, 25, 6085−6091

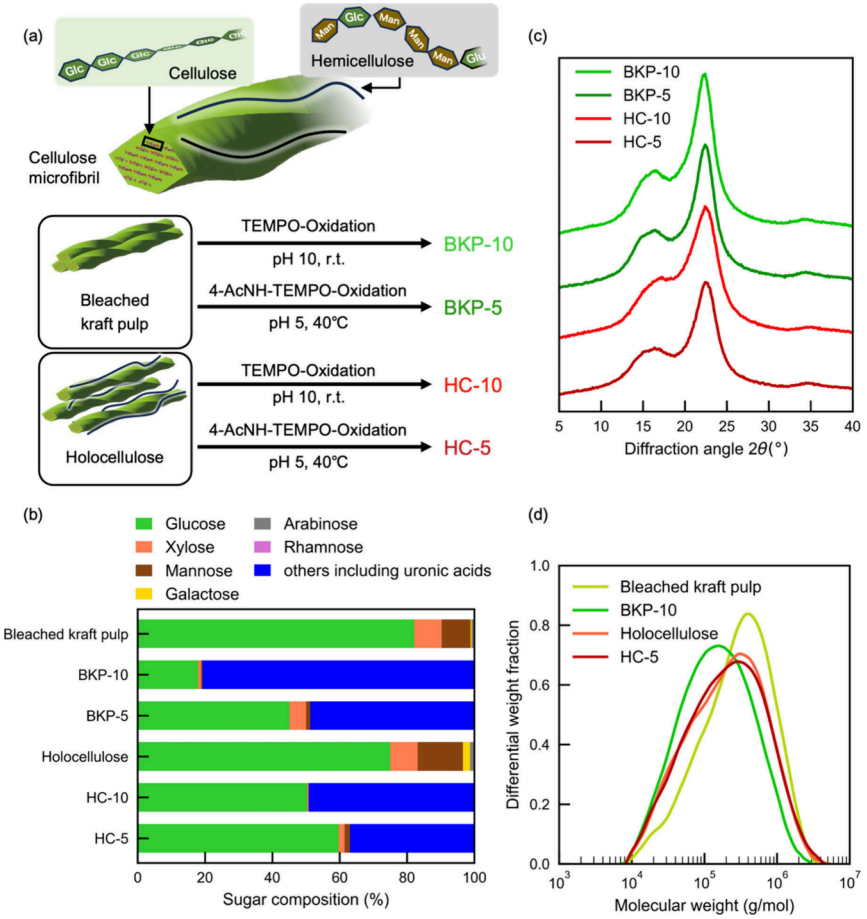

Figure 1. CNF preparation. (a) Raw materials and pH during oxidation for the four types of CNFs in this study. The terms Glc and Man indicate glucose and mannose, respectively. (b) Sugar composition analysis of the raw materials and CNFs. (c) WAXD profiles of the oxidized raw materials. (d) Molecular weight distributions of the raw materials and two CNFs.

as a catalyst at alkaline pH 10 is often utilized.[16] This process efficiently introduces carboxy groups onto the surface of microfibrils within several hours but significantly reduces the molecular weight of the cellulose through a side reaction.[15,17]

The use of another TEMPO oxidation system at a weakly acidic pH for producing CNF dispersions of microfibril units while inhibiting depolymerization of cellulose has been proposed. Tanaka et al.[18] demonstrated that CNFs produced via 4-acetamido-TEMPO (4-AcNH-TEMPO) oxidation of bleached kraft pulp at pH 5 have a distinctly higher molecular weight than CNFs produced via TEMPO oxidation at neutral pH 7 or alkaline pH 10. Kuramae et al.[19] produced CNFs from holocelluloses via TEMPO oxidation at pH 7. However, 4-AcNH-TEMPO oxidation at pH 5 has never been applied to holocelluloses. Note also that there are still no reports on quantitative analysis of defects for any CNFs produced from holocelluloses.

In a previous work, we constructed an atomic force microscopy (AFM) image processing program that statistically analyzes CNF defects such as dents and kinks.[3] In this study, we utilized this program to comprehensively analyze the correlations between the defect density of CNFs and either the raw material species or the TEMPO oxidation conditions. Softwood bleached kraft pulp and softwood holocellulose were chosen as the raw materials. These two raw materials were subjected to the 4-AcNH-TEMPO oxidation reaction at pH 5 or the TEMPO oxidation at pH 10 to prepare four types of CNFs. Based on the defect analysis of these CNFs, we found a process that produces defectless CNF dispersions comprising single microfibril units of the highest quality to our knowledge.

A signal processing (wavelet transform) was also applied to the AFM height profiles of the CNFs to analyze the location and periodicity of twist in the CNFs. This study is the first attempt at statistically analyzing the relationship between the defects and twist of CNFs.

Four types of CNFs were prepared from bleached kraft pulp oxidized at pH 10, bleached kraft pulp oxidized at pH 5, holocellulose oxidized at pH 10, and holocellulose oxidized at pH 5, which are hereafter denoted BKP-10, BKP-5, HC-10, and HC-5, respectively (Figure 1a). The carboxy group contents of BKP-10, BKP-5, HC-10, and HC-5 were approximately 1.7, 1.2, 1.5, and 1.1 mmol/g, respectively. The results of the sugar composition analysis of the series of samples are shown in Figure 1b. The major neutral sugars of hemicelluloses in both the bleached kraft pulp and holocellulose were mannose and xylose. Assuming that softwood glucomannan has a sugar composition of mannose:glucose = 3:1,[20,21] the bleached kraft pulp and holocellulose used in this study were estimated to contain approximately 20% and 30% hemicelluloses, respectively. Most hemicelluloses were leached out in the oxidation−purification process,[19,22] so the hemicellulose contents of the CNF samples were approximately 1−5%. Acidic sugars were not detectable by the sugar composition analysis adopted in this study.

https://doi.org/10.1021/acs.nanolett.4c06483
Nano Lett. 2025, 25, 6085−6091

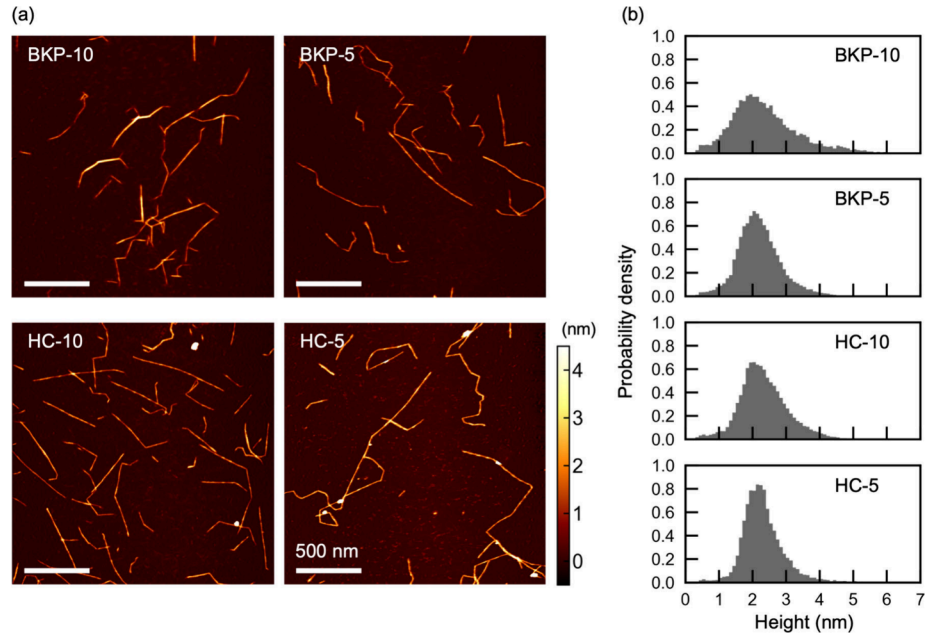

Figure 2. AFM height analysis. (a) AFM height images and (b) height distributions of the four types of CNFs.

Therefore, the glucuronate units introduced to the microfibril surface via oxidation were included in the "others" category. These results indicate that the CNF samples prepared in this study had a high cellulose purity.

Figure 1c shows wide-angle X-ray diffraction (WAXD) patterns of the oxidized raw materials before disintegration. Compared with the pulp samples (BKP-5, 10), the holocellulose samples (HC-5, 10) presented broad diffraction patterns. Considering (1) the minor hemicellulose contents in the oxidized samples and (2) the positive correlation between the aggregate density of microfibrils and the X-ray diffraction intensity,[23] these results suggest that fibril aggregation within the holocellulose was suppressed compared with that in the pulp, as previously reported.[23]

Figure 1d shows the molecular weight distributions of the bleached kraft pulp, the holocellulose, BKP-10, and HC-5. Their weight-average molecular weights were 458000, 377000, 262000, and 381000 g/mol, respectively. The holocellulose had a slightly lower average molecular weight than the bleached kraft pulp,[24] probably because the holocellulose contained more low-molecular-weight hemicelluloses.[25] In the comparison of the CNF samples with a high cellulose purity, HC-5 had a distinctly higher molecular weight than BKP-10. Additionally, the molecular weight of the bleached kraft pulp was significantly lowered by the oxidation−disintegration process, whereas the average molecular weight of the holocellulose was slightly increased by a similar process. This change in the molecular weight of holocellulose can be interpreted as the result of leaching of hemicelluloses (Figure 1b) and of the increase in the molecular weight due to oxidation of anhydroglucose units to glucuronate units.[26]

A defect growth process was proposed: dent defects are formed on CNFs at the beginning stage of disintegration, and these dents induce further deformations such as kinks and fracture in the subsequent mechanical shearing process.[3] In this study, we thus focused on dents as the origin of diverse defects and quantified the length of the dent parts along the CNFs.

Figure 2a shows typical AFM images of each CNF. Tracing the entire length of the CNFs in the AFM images was difficult, especially for HC-5, due to the limited scope of AFM and the entanglement of the CNFs. We thus estimated the average lengths of the CNFs from viscosity using an empirical equation for the correlation between the rheological behavior of the CNF dispersions and the average lengths of the CNFs determined via microscopy, according to a previous report.[27] The average lengths of BKP-10, BKP-5, HC-10, and HC-5 thus estimated were approximately 0.6, 1.0, 1.1, and 2.1 μm, respectively. The measured intrinsic viscosities are listed in Table S1.

The AFM height distributions of the CNFs were analyzed using a modified version of the self-made software used in a previous study (Figure 2b).[3] The modes of the height distributions for BKP-10, BKP-5, HC-10, and HC-5 were 1.95, 2.05, 1.95, and 2.15 nm, respectively. The 95% confidence intervals for the modes of each sample, obtained using the bootstrap method, are shown in Table S2. Although the differences were small, BKP-10 had the smallest mode, while HC-5 had the largest. As observed in the AFM images, BKP-10 contained both thick and thin fibrils and exhibited a broad height distribution. In contrast, the HC-5 fibrils were homogeneous, and their height distribution was narrow. The height distributions of BKP-5 and HC-10 were similar in shape.

Assuming the 18-chain models reported thus far, in which a single microfibril comprises 18 molecular chains of cellulose but has several possibilities for its cross-sectional shape,[23,28] the cross-sectional dimensions of CNFs dispersed as microfibril units are within the range of 2.09−3.75 nm. Considering both the compressive moduli of the CNFs in the cross-sectional direction (~30 GPa)[29] and the AFM settings adopted in this study, the indentation of the AFM tip into a CNF was estimated to be approximately 0.1 nm at most.[3] Thus, the range of the AFM height distribution of single CNFs was considered to be from approximately 1.9 to 3.7 nm. Thus, we classified the AFM heights into three categories: 0 to less than 1.9 nm, 1.9 to less than 3.7 nm, and 3.7 nm or more. The

https://doi.org/10.1021/acs.nanolett.4c06483
Nano Lett. 2025, 25, 6085−6091

height components of less than 1.9 nm, detected as dent defects, were highlighted in blue on the AFM images (Figure 3a). BKP-10 had long defects that were widely distributed,

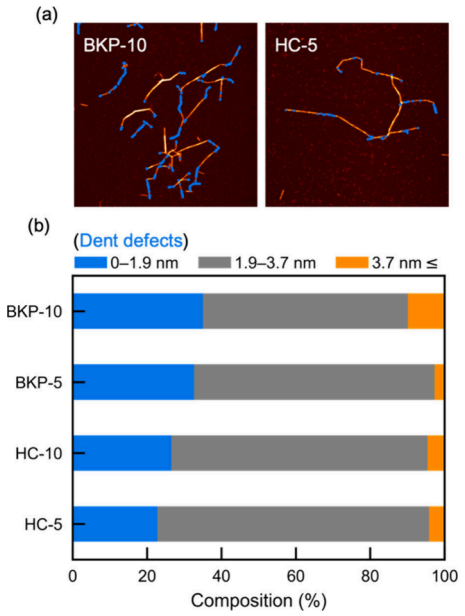

Figure 3. Defect analysis. (a) Distributions of dent defects on two types of CNFs. The dent defects are represented in blue. (b) Defect ratios of each CNF.

whereas HC-5 exhibited shorter defects that were more locally confined. This trend is further supported by the scatter plot of defect length and depth (Figure S1), which quantitatively demonstrates that HC-5 has smaller dent defects compared to BKP-10. The ratios of these dent regions were approximately 35%, 33%, 27%, and 23% for BKP-10, BKP-5, HC-10, and HC-5, respectively (Figure 3b). Compared with the BKP series, the HC series had fewer and smaller defects under the same pH conditions. For the same raw material, the CNFs at pH 5 (BKP-5 and HC-5) had slightly fewer and smaller defects than the CNFs at pH 10 (BKP-10 and HC-10).

These results indicate that both factors we speculated to influence defect formation—raw materials and oxidation conditions—affected its formation. In our previous study, we proposed a mechanism in which dent defects are generated during mechanical disintegration due to the detachment of molecular chains from the CNF surface.[3] A key factor influencing this detachment is the presence of hemicellulose, which coats the microfibril surface in the pulp.[13−15] Since hemicellulose forms a protective layer around the fibrils, its presence likely reduces molecular chain detachment, thereby suppressing dent defect formation in the HC series. Another factor is the pH condition during TEMPO oxidation. Under mildly acidic conditions, oxidative degradation of cellulose at the fibril surface is known to be suppressed, leading to reduced detachment of molecular chains.[18]

We also demonstrated the WAXD and solid-state ^{13}C NMR analyses of defect-rich BKP-10 and defectless HC-5 CNFs to compare their crystallinity. In both WAXD and solid-state ^{13}C NMR spectra, HC-5 showed sharper peaks than BKP-10 (Figure S2). The difference was particularly noticeable in the NMR data, where the C4 crystallinity index was 13% for BKP-10 and 20% for HC-5. These results indicate that CNFs with fewer defects exhibit higher crystallinity. The dent defects in the CNFs, which are caused by molecular chain detachment from the surface, result in smaller crystalline size, leading to a decrease in crystallinity.

CNFs have been reported to exhibit right-handed twist, which is observed as periodic height variations along the fiber axis in AFM images.[4,30] Among the CNFs prepared in this study, twist was more frequently and clearly observed in HC-5 with fewer defects than in BKP-10 with more defects (Figure 2). Therefore, we conducted a statistical analysis to investigate the relationship between the defect structure and the twist behavior of the CNFs.

We employed the wavelet transform to analyze the twist of the CNFs. The wavelet transform is a method for determining which frequencies are present at specific positions within data. For example, it was applied to the height profile extracted from the AFM image of a CNF exhibiting twist (Figure 4a). This analysis yielded a wavelet power spectrum (Figure 4b), where the horizontal axis represents the position along the fiber, and the vertical axis corresponds to the frequency, which represents the twist pitch in this case. The brightest areas in the spectrum indicate strong periodicity, and the most prominent periodicity, shown in yellow, appears within the range of 64−128 nm. This result matches the periodic height variation, with a twist pitch of approximately 100 nm, observed in the height profile. To determine the presence of twist, the strength of the periodicity was quantified using the scale-averaged power, and positions with statistically significant periodicity were identified according to the method of Torrence and Compo (Figure 4c).[31] The scale-averaged power was calculated over the range of 32−128 nm, with reference to the previously reported twist pitch of CNFs. Finally, at each position where twist was detected, the frequency with the strongest periodicity was extracted (red lines in Figure 4b), and these frequencies were used as the twist pitch of the CNF at each location.

Assuming the 18-chain model, the detected twist pitch corresponds to a 180° rotation (Figure 4d). We applied the above method to a height profile based on the 18-chain model, assuming a constant twist pitch of 100 nm, and confirmed the successful detection of a 100 nm twist pitch (Figure 4e).

Using the above method, the ratio of the length detected as being twisted to the total length of the CNF was calculated (Figure 5a). The twist ratios for BKP-10, BKP-5, HC-10, and HC-5 were 4.93%, 11.13%, 11.51%, and 23.59%, respectively, indicating that CNFs with fewer defects had more twisted regions. Figure 5b shows the distribution of the twist pitch of HC-5 (see Figure S5 for the twist pitch distributions of BKP-10, BKP-5, and HC-10). A broad distribution ranging from 50 to 120 nm was observed for all the CNF samples.

Four potential factors may explain why more twisting was detected in the CNFs with fewer defects. The first factor is the length of the CNFs. For short CNFs less than 100 nm, the frequency analysis resolution decreases, making detection of periodicity difficult even if twist is present. The second factor is the irregular fluctuation of the height profile caused by defects. Because previous studies suggested that CNFs tend to delaminate along the (200) and (1−10) planes, we assumed a model in which two molecular layers are delaminated with a 40% probability from the (200) and (1−10) cross-sectional planes.[32,33] The height profile of a CNF with such delamination was simulated, but a constant twist pitch shows an irregular periodicity. As a result, fewer regions were identified as having statistically significant twist (Figure S3b). Similar CNFs were observed in the actual data (Figure S4).

https://doi.org/10.1021/acs.nanolett.4c06483
Nano Lett. 2025, 25, 6085−6091

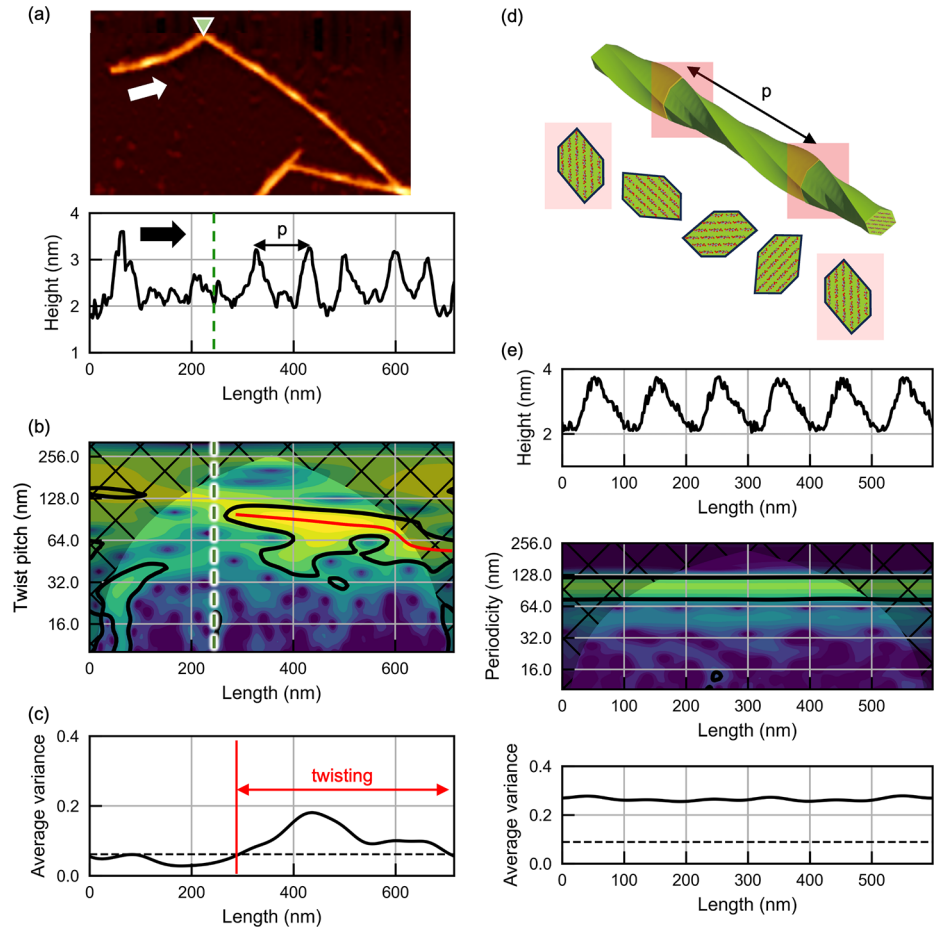

Figure 4. Wavelet transform of the height profile of a twisted HC-5 CNF. (a) AFM image of the twisted CNF and its height profile, where the kink positions are indicated by green arrowheads. (b) Wavelet power spectrum of the height profile shown in part a obtained using the Morlet wavelet. (c) Scale-averaged wavelet power over the 32−128 nm periodicity range. The solid and dashed lines in parts b and c represent the 95% confidence level assuming red noise. (d) An 18-chain CNF cross-sectional model, where the twist pitch p is indicated. (e) Simulated height profile of the twisted CNF and its wavelet transform.

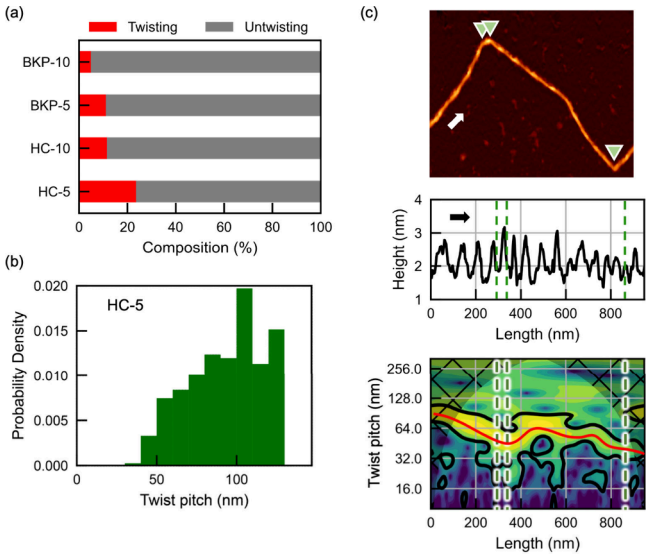

Figure 5. Composition and pitch of CNF twist. (a) Composition percentages of the length of the twisted section to the total length of the CNF. (b) Distribution of the twist pitch for HC-5. (c) AFM image and transform result for a twisted CNF with kinks. The green arrowheads and dashed lines correspond to the kink positions.

This suggests that even if a CNF is periodically twisted, defects can hinder the detection of twist. The third factor is the possibility that defects disrupt or suppress the twist periodicity itself. Although this phenomenon cannot be directly confirmed from the AFM data, previous studies reported that the driving force of CNF twisting is intramolecular hydrogen bonding and that the twist period correlates with the fibril width.[34−36] Therefore, dent defects are highly likely to disrupt the twist periodicity of CNFs. The fourth factor is the difference in the carboxy group content on the surface of the CNFs. Previous studies have reported that CNFs can undergo structural rearrangement, including untwisting, due to interactions with the substrate during drying.[37,38] Given this, such interactions may be influenced by the carboxy group content, thereby affecting the degree of twisting.

The twist pitches obtained in this study include the range previously reported for TEMPO-oxidized CNFs (approximately 40−70 nm) but show greater variability.[30] One possible reason for this is that our method detected twist even in regions with significant noise, which may have been overlooked by previous analyses that measured the distances between peaks (Figure S6). Furthermore, as shown in Figure 5c, twist was also detected in areas where the pitch fluctuated near kinks, contributing to the broader distribution of pitches.

https://doi.org/10.1021/acs.nanolett.4c06483
Nano Lett. 2025, 25, 6085−6091

This study is the first to demonstrate that the raw material selection and chemical pretreatment in CNF preparation are critical for controlling defects in single CNFs. Defectless CNFs were obtained by using weakly aggregating holocellulose as a raw material and applying TEMPO oxidation under weakly acidic conditions, which suppressed the decomposition reactions. These defectless CNFs are characterized by their long length, with mechanical breakdown into smaller CNFs effectively suppressed, and by their highly uniform height owing to the minimal presence of dent defects and aggregation. Moreover, CNFs with fewer defects exhibit more frequent periodic height variations associated with twist. This finding suggests that the extent of detectable twist in CNF samples could serve as an indicator for evaluating their quality.

Establishing a method to control defects allows maximization of the potential of CNFs and facilitates the design of higher-performance CNF materials. In particular, defect suppression is expected to significantly enhance their performance as reinforcement materials. Additionally, these CNFs are expected to closely maintain the native state of cellulose, contributing to a better understanding of the structure of individual cellulose microfibrils, which remains largely unexplored.

■ ASSOCIATED CONTENT

Data Availability Statement

The Python code for the calculation of the theoretical height range of CNFs is provided on GitHub (https://github.com/terio0819/AFM_Simulation/tree/main).

Supporting Information

The Supporting Information is available free of charge at https://pubs.acs.org/doi/10.1021/acs.nanolett.4c06483.

Experimenta section, experimental intrinsic viscosity $[\eta]_e$ values of each CNF (Table S1), 95% confidence intervals for the height modes of each sample (Table S2), average length and depth of dent defects for each sample (Figure S1), WAXD profilea and NMR spectra of BKP-10 and HC-5 (Figure S2), simulated wavelet transform (Figure S3), twist pitch distributions of BKP-10, BKP-5, and HC-10 (Figure S4), wavelet transform of a CNF for which no twist can be detected (Figure S5), detection of the ambiguous twist of a CNF using the wavelet transform (Figure S6), simulated height range of CNFs (Figure S7), calculation of CNF indentation by the AFM tip (Figure S8), and Fourier transform of a nontwisted CNF (Figure S9) (PDF)

■ AUTHOR INFORMATION

Corresponding Authors

Tsuguyuki Saito − *Department of Biomaterial Sciences, Graduate School of Agricultural and Life Sciences, The University of Tokyo, Bunkyo-ku, Tokyo 113-8657, Japan;* orcid.org/0000-0003-1073-6663; Email: saitot@g.ecc.u-tokyo.ac.jp

Kayoko Kobayashi − *Division of Forest and Biomaterials Science, Graduate School of Agriculture, Kyoto University, Sakyo-ku, Kyoto 606-8502, Japan;* orcid.org/0000-0003-0459-7900; Email: kobayashi.kayoko.3s@kyoto-u.ac.jp

Authors

Tomoki Ito − *Department of Biomaterial Sciences, Graduate School of Agricultural and Life Sciences, The University of Tokyo, Bunkyo-ku, Tokyo 113-8657, Japan;* orcid.org/0000-0002-2473-7117

Kazuho Daicho − *Institute of Engineering Innovation, School of Engineering, University of Tokyo, Bunkyo-ku, Tokyo 113-8656, Japan;* orcid.org/0000-0003-4203-2257

Shuji Fujisawa − *Department of Biomaterial Sciences, Graduate School of Agricultural and Life Sciences, The University of Tokyo, Bunkyo-ku, Tokyo 113-8657, Japan;* orcid.org/0000-0002-5221-6781

Complete contact information is available at: https://pubs.acs.org/10.1021/acs.nanolett.4c06483

Author Contributions

T.S. and K.K. conceived the concept of the study and designed the experiments. T.I. and K.D. performed the experiments, and all the authors analyzed the data. T.I. primarily wrote the Python code with K.K. T.I. prepared the first version of the manuscript, and K.D., T.S., and K.K. revised the manuscript with contributions from all the authors.

Notes

The authors declare no competing financial interest.

■ ACKNOWLEDGMENTS

This research was supported by a Grant-in-Aid for Young Scientists (Grant 23KJ0523 to T.I.), Grants-in-Aid for Scientific Research (Grant 21H04733 to T.S. and K.K., Grant 22KJ1473 to K.D., and Grant JP23H02270 to S.F.) from the Japan Society for the Promotion of Science, JST CREST (Grant JPMJCR22L3 to T.S., K.K., and S.F.), and JST ASPIRE (Grant JPMJAP2310 to T.S.) from the Japan Science and Technology Agency (JST).

■ REFERENCES

(1) Li, T.; Chen, C.; Brozena, A. H.; Zhu, J. Y.; Xu, L.; Driemeier, C.; Dai, J.; Rojas, O. J.; Isogai, A.; Wågberg, L.; Hu, L. Developing Fibrillated Cellulose as a Sustainable Technological Material. *Nature* **2021**, *590* (7844), 47−56.

(2) Lim, J. H.; Jing, Y.; Park, S.; Nishiyama, Y.; Veron, M.; Rauch, E.; Ogawa, Y. Structural Anisotropy Governs the Kink Formation in Cellulose Nanocrystals. *J. Phys. Chem. Lett.* **2023**, *14*, 3961−3969.

(3) Ito, T.; Daicho, K.; Fujisawa, S.; Saito, T.; Kobayashi, K. Atomic-Scale Dents on Cellulose Nanofibers: The Origin of Diverse Defects in Sustainable Fibrillar Materials. *Nanoscale Horiz* **2022**, *7* (10), 1186−1191.

(4) Usov, I.; Nyström, G.; Adamcik, J.; Handschin, S.; Schütz, C.; Fall, A.; Bergström, L.; Mezzenga, R. Understanding Nanocellulose Chirality and Structure-Properties Relationship at the Single Fibril Level. *Nat. Commun.* **2015**, *6* (1), 7564.

(5) Ciesielski, P. N.; Wagner, R.; Bharadwaj, V. S.; Killgore, J.; Mittal, A.; Beckham, G. T.; Decker, S. R.; Himmel, M. E.; Crowley, M. F. Nanomechanics of Cellulose Deformation Reveal Molecular Defects That Facilitate Natural Deconstruction. *Proc. Natl. Acad. Sci. U. S. A.* **2019**, *116* (20), 9825−9830.

(6) Martoïa, F.; Dumont, P. J. J.; Orgéas, L.; Belgacem, M. N.; Putaux, J.-L. On the Origins of the Elasticity of Cellulose Nanofiber Nanocomposites and Nanopapers: A Micromechanical Approach. *RSC Adv.* **2016**, *6* (53), 47258−47271.

(7) Pennells, J.; Godwin, I. D.; Amiralian, N.; Martin, D. J. Trends in the Production of Cellulose Nanofibers from Non-Wood Sources. *Cellulose* **2020**, *27* (2), 575−593.

(8) Kargupta, W.; Seifert, R.; Martinez, M.; Olson, J.; Tanner, J.; Batchelor, W. Sustainable Production Process of Mechanically Prepared Nanocellulose from Hardwood and Softwood: A Comparative Investigation of Refining Energy Consumption at Laboratory and Pilot Scale. *Ind. Crops Prod.* **2021**, *171*, 113868.

(9) Sanchez-Salvador, J. L.; Campano, C.; Balea, A.; Tarrés, Q.; Delgado-Aguilar, M.; Mutjé, P.; Blanco, A.; Negro, C. Critical Comparison of the Properties of Cellulose Nanofibers Produced from Softwood and Hardwood through Enzymatic, Chemical and Mechanical Processes. *Int. J. Biol. Macromol.* **2022**, *205*, 220−230.
(10) Duchesne, I.; Takabe, K.; Daniel, G. Ultrastructural Localisation of Glucomannan in Kraft Pulp Fibres. *Holzforschung* **2003**, *57* (1), 62−68.
(11) Turbak, A.; Snyder, F. W.; Sandberg, K. R. Microfibrillated Cellulose, A New Cellulose Product: Properties, Uses, and Commercial Potential. *J. Appl. Polym. Sci., Appl. Polym. Symp.* **1983**, *37*, 815.
(12) Chaker, A.; Alila, S.; Mutjé, P.; Vilar, M. R.; Boufi, S. Key Role of the Hemicellulose Content and the Cell Morphology on the Nanofibrillation Effectiveness of Cellulose Pulps. *Cellulose* **2013**, *20* (6), 2863−2875.
(13) Iwamoto, S.; Abe, K.; Yano, H. The Effect of Hemicelluloses on Wood Pulp Nanofibrillation and Nanofiber Network Characteristics. *Biomacromolecules* **2008**, *9* (3), 1022−1026.
(14) Hult, E.-L. Characterization of the Supermolecular Structure of Cellulose in Wood Pulp Fibres. *Cellulose* **2003**, *10* (2), 103−110.
(15) Yang, X.; Reid, M. S.; Olsén, P. O.; Berglund, L. A. Eco-Friendly Cellulose Nanofibrils Designed by Nature: Effects from Preserving Native State. *ACS Nano* **2020**, *14*, 724.
(16) Saito, T.; Nishiyama, Y.; Putaux, J.-L.; Vignon, M.; Isogai, A. Homogeneous Suspensions of Individualized Microfibrils from TEMPO-Catalyzed Oxidation of Native Cellulose. *Biomacromolecules* **2006**, *7* (6), 1687−1691.
(17) Hiraoki, R.; Fukuzumi, H.; Ono, Y.; Saito, T.; Isogai, A. SEC-MALLS Analysis of TEMPO-Oxidized Celluloses Using Methylation of Carboxyl Groups. *Cellulose* **2014**, *21* (1), 167−176.
(18) Tanaka, R.; Saito, T.; Isogai, A. Cellulose Nanofibrils Prepared from Softwood Cellulose by TEMPO/NaClO/$NaClO_2$ Systems in Water at PH 4.8 or 6.8. *Int. J. Biol. Macromol.* **2012**, *51* (3), 228−234.
(19) Kuramae, R.; Saito, T.; Isogai, A. TEMPO-Oxidized Cellulose Nanofibrils Prepared from Various Plant Holocelluloses. *React. Funct. Polym.* **2014**, *85*, 126−133.
(20) Gyaw, M. O.; Timell, T. E. Constitution of a Glucomannan from the Wood of Eastern White Pine (Pinus Strobus l.). *Can. J. Chem.* **1960**, *38* (10), 1957−1966.
(21) De, K. K.; Timell, T. E. The Acid Hydrolysis of Glycosides. *Carbohydr. Res.* **1967**, *4* (1), 72−77.
(22) Hiraoki, R.; Ono, Y.; Saito, T.; Isogai, A. Molecular Mass and Molecular-Mass Distribution of TEMPO-Oxidized Celluloses and TEMPO-Oxidized Cellulose Nanofibrils. *Biomacromolecules* **2015**, *16* (2), 675−681.
(23) Daicho, K.; Saito, T.; Fujisawa, S.; Isogai, A. The Crystallinity of Nanocellulose: Dispersion-Induced Disordering of the Grain Boundary in Biologically Structured Cellulose. *ACS Appl. Nano Mater.* **2018**, *1* (10), 5774−5785.
(24) Ono, Y.; Funahashi, R.; Saito, T.; Isogai, A. Investigation of Stability of Branched Structures in Softwood Cellulose Using SEC/MALLS/RI/UV and Sugar Composition Analyses. *Cellulose* **2018**, *25* (4), 2667−2679.
(25) Ono, Y.; Hiraoki, R.; Fujisawa, S.; Saito, T.; Isogai, A. SEC-MALLS Analysis of Wood Holocelluloses Dissolved in 8% LiCl/1,3-Dimethyl-2-Imidazolidinone: Challenges and Suitable Analytical Conditions. *Cellulose* **2015**, *22* (5), 3347−3357.
(26) Daicho, K.; Kobayashi, K.; Fujisawa, S.; Saito, T. Crystallinity-Independent yet Modification-Dependent True Density of Nanocellulose. *Biomacromolecules* **2020**, *21* (2), 939−945.
(27) Tanaka, R.; Saito, T.; Ishii, D.; Isogai, A. Determination of Nanocellulose Fibril Length by Shear Viscosity Measurement. *Cellulose* **2014**, *21* (3), 1581−1589.
(28) Rosén, T. R.; He, H.; Wang, R.; Zhan, C.; Chodankar, S.; Fall, A.; Aulin, C.; Larsson, T.; Lindström, T.; Hsiao, B. S. Cross-Sections of Nanocellulose from Wood Analyzed by Quantized Polydispersity of Elementary Microfibrils. *ACS Nano* **2020**, *14*, 16743−16754.
(29) Moon, R. J.; Martini, A.; Nairn, J.; Simonsen, J.; Youngblood, J. Cellulose Nanomaterials Review: Structure, Properties and Nanocomposites. *Chem. Soc. Rev.* **2011**, *40*, 3941−3994.
(30) Arcari, M.; Zuccarella, E.; Axelrod, R.; Adamcik, J.; Sánchez-Ferrer, A.; Mezzenga, R.; Nyström, G. Nanostructural Properties and Twist Periodicity of Cellulose Nanofibrils with Variable Charge Density. *Biomacromolecules* **2019**, *20* (3), 1288−1296.
(31) Torrence, C.; Compo, G. P. A Practical Guide to Wavelet Analysis. *Bull. Am. Meteorol. Soc.* **1998**, *79* (1), 61−78.
(32) Li, Q.; Renneckar, S. Supramolecular Structure Characterization of Molecularly Thin Cellulose I Nanoparticles. *Biomacromolecules* **2011**, *12* (3), 650−659.
(33) Su, Y.; Burger, C.; Ma, H.; Chu, B.; Hsiao, B. S. Exploring the Nature of Cellulose Microfibrils. *Biomacromolecules* **2015**, *16* (4), 1201−1209.
(34) Bu, L.; Himmel, M. E.; Crowley, M. F. The Molecular Origins of Twist in Cellulose I-Beta. *Carbohydr. Polym.* **2015**, *125*, 146−152.
(35) Zhao, Z.; Shklyaev, O. E.; Nili, A.; Mohamed, M. N. A.; Kubicki, J. D.; Crespi, V. H.; Zhong, L. Cellulose Microfibril Twist, Mechanics, and Implication for Cellulose Biosynthesis. *J. Phys. Chem. A* **2013**, *117* (12), 2580−2589.
(36) Willhammar, T.; Daicho, K.; Johnstone, D. N.; Kobayashi, K.; Liu, Y.; Midgley, P. A.; Bergström, L.; Saito, T. Local Crystallinity in Twisted Cellulose Nanofibers. *ACS Nano* **2021**, *15* (2), 2730−2737.
(37) Ogawa, Y. Electron Microdiffraction Reveals the Nanoscale Twist Geometry of Cellulose Nanocrystals. *Nanoscale* **2019**, *11* (45), 21767−21774.
(38) Kong, L.; Alqus, R.; Yong, C. W.; Todorov, I.; Eichhorn, S. J.; Bryce, R. A. Cellulose Iβ Microfibril Interaction with Pristine Graphene in Water: Effects of Amphiphilicity by Molecular Simulation. *J. Mol. Graph. Model.* **2023**, *118*, 108336.

https://doi.org/10.1021/acs.nanolett.4c06483
Nano Lett. 2025, 25, 6085−6091